International Journal of Heat and Mass Transfer 121 (2018) 402–411

Contents lists available at ScienceDirect

International Journal of Heat and Mass Transfer

journal homepage: www.elsevier.com/locate/ijhmt

Numerical investigation of droplet spreading and heat transfer on hot substrates

Yongpan Cheng [a,b,*], Fan Wang [b], Jinliang Xu [a,*], Dong Liu [a], Yi Sui [b]

[a] Beijing Key Laboratory of Multiphase Flow and Heat Transfer for Low Grade Energy, North China Electric Power University, Beijing 102206, China
[b] School of Engineering and Materials Science, Queen Mary University of London, Mile End Road, London E1 4NS, United Kingdom

ARTICLE INFO

Article history:
Received 7 September 2017
Received in revised form 31 December 2017
Accepted 5 January 2018

Keywords:
Spray cooling
Droplet spreading
Multiphase flows
Molecular kinetic theory
Level set method

ABSTRACT

Droplet spray cooling has wide applications in electronic cooling, steam generators, evaporators and condensers etc due to its high efficiency. The cooling effect depends on the droplet spreading dynamics greatly. In our study the transient two-dimensional axisymmetric model for droplet cooling is developed with a level set method, where the dynamics of the moving contact line is described with the Molecular Kinetic Theory (MKT). After validation with experimental data, the effect of impact velocity, surface tension, initial droplet radius, equilibrium contact angle and liquid viscosity on droplet spreading is investigated. It is found that the dynamics of the moving contact line can be described accurately with MKT, and the predicted droplet spreading radius agrees quite well with the experimental data, while the Constant Contact Angle (CCA) model overpredicts the droplet spreading rate. The maximum heat flux occurs at the point when the droplet spreading transits from capillary-inertial spreading to capillary-viscous spreading. The droplet spreading rate will increase with the increasing impact velocity, surface tension and initial radius, or decreasing equilibrium contact angle and liquid viscosity. Due to the effect of thermo-capillary force, the cold substrate can promote the droplet spreading, and the hot substrate can retard the droplet spreading. These findings may be of great significance for effective droplet spreading cooling.

1. Introduction

Spray cooling is an effective way for rapid heat removal from the solid surfaces, it is widely used in electric cooling [1], steam generators, liquid evaporators, condensers in industry [2]; furthermore, it can also be used in medicine to cool down the outer layer of the human skin during dermatological laser treatments [3]. During spray cooling there are mainly two distinct stages, named the initial spreading stage and the later evaporation stage [4]. Although the spreading stage is much shorter than the evaporation stage, and the amount of heat transfer during this stage is insignificant, the initial droplet spreading has substantial effect on the liquid coverage and the subsequent evaporation heat transfer [5], hence comprehensive studies have been carried out in this area.

Pasandideh-Fard et al. [6] studied the water droplet impinging cooling on a hot surface, they revealed that increasing impact velocity can enhance the heat flux from the substrate by only a small amount, due to the effect that the wetting area for heat transfer is not increased too much under high impact velocity. They also found that at a fixed Reynolds number the cooling efficiency increases with Weber number, however, at large Weber numbers, the cooling efficiency depends only on the Prandtl number, independent of the droplet impact velocity or size. Moon et al. [7] studied the effect of wetting states (i.e., non-wetting, partial-wetting and total-wetting) on the heat transfer of an impinging droplet on textured substrate; they also examined the effect of impact Weber number, surface temperature and textured area fraction on the heat transfer. They further studied the spreading and receding characteristics of a non-Newtonian droplet impinging on a heated surface [8], and found that the maximum spreading diameter for a Newtonian DI-water droplet is larger than that of a non-Newtonian droplet because of the difference in liquid viscosity. In the spreading regime, the dynamic contact angle is almost similar for the Newtonian and non-Newtonian droplets, but in the receding regime, it substantially changes with temperature due to the variation of viscosity with temperature. Ganesan et al. [9] investigated the non-isothermal droplet impact on a heated solid substrate with circular heterogeneous wettability. The heterogeneous wettability was incorporated into the arbitrary

* Corresponding authors at: Beijing Key Laboratory of Multiphase Flow and Heat Transfer for Low Grade Energy, North China Electric Power University, Beijing 102206, China, (Y. Cheng).
E-mail addresses: chengyp@ncepu.edu.cn (Y. Cheng), xjl@ncepu.edu.cn (J. Xu).

https://doi.org/10.1016/j.ijheatmasstransfer.2018.01.026
0017-9310/

Nomenclature

A	fitting parameter
B	fitting parameter
Bo	Bond number
Ca	Capillary number
C_p	non-dimensional specific heat, $C_p = H + (1-H)C_{p,g}/C_{p,l}$
H	Heaviside function
k°	equilibrium frequency of molecular displacement
k_B	Boltzmann constant
Ma	Marangoni number
n	number of sites of solid-liquid interaction per unit area
$\vec{n}$	normal vector
Nu	Nusselt number
Oh	Ohnesorge number
p	non-dimensional pressure
r	ratio
r_0	droplet radius
Re	Reynolds number
t	non-dimensional time
T	non-dimensional temperature
u	non-dimensional velocity
We	Weber number
x, y	coordinates
δ	dirac delta function
ε	non-dimensional thickness of interface
ϕ	distance function
λ	non-dimensional thermal conductivity $\lambda = H + (1-H)\lambda_g/\lambda_l$. Distance between adsorption sites on the solid surface
κ	curvature
μ	non-dimensional viscosity, $\mu = H + (1-H)\mu_g/\mu_l$
θ	contact angle
ρ	non-dimensional average density, $\rho = H + (1-H)\rho_g/\rho_l$
ρ_0	density
σ_0	surface tension
σ_T	variation coefficient of surface tension over temperature
ci	capillary-inertial
cl	contact line
d	density, dynamic
g	gas
l	liquid
s	surface
w	wall

Lagrangian-Eulerian (ALE) model through the space-dependent contact angle. They found that the equilibrium position depends on the wettability contrast and the diameter of the inner circular patterned region, the heat transfer is higher at smaller wettability contrast or larger inner patterned region. The total heat transfer increases with increasing impact Weber number. They also adopted the dynamic contact angle with variation of local temperature, and studied droplet impact dynamics and heat transfer under different values of Reynolds number, Weber number, solid phase initial temperature and reference equilibrium contact angle [10]. They found that the temperature-dependent contact angle is negligible in partially wetting droplets, but it becomes essential for non-wetting and highly wetting droplet impact.

Berberovic et al. [2] studied the impact heat transfer of a cold liquid droplet onto a dry heated substrate, the thermophysical properties of droplets varies with temperature. In their computational model based on the volume of fluid method, the air flow surrounding the liquid droplet was considered; the numerical results agree quite well with experimental and theoretical results in terms of droplet spreading pattern, associated heat flux and temperature distribution. Diaz and Orgega [11] investigated the gas-propelled liquid droplet impinging onto a heated surface through numerical simulation; the volume of fluid model was adopted with a constant contact angle. They found that the heat transfer is mainly dominated by diffusion during the early stage of impact. The heat transfer enhancement is expected to occur when the ratio of kinetic energy of carrier gas over droplet is larger than 0.1. Strotos et al. [12] studied the water droplet impinging cooling with volume of fluid method, in this model the droplet dynamics, heat conduction in solid substrate and droplet evaporation were coupled together, the predicted droplet shape, temperature, flow and vapor distribution agree well with experimental observations. They also summarized the non-dimensional parameters for predicting the cooling effectiveness of droplet impinging on the solid surfaces [13]. Bhardwaj et al. [14] numerically studied the influence of liquid properties and interfacial heat transfer during microdroplet deposition onto a glass substrate. Four liquids (i.e., isopropanol, water, dielectric fluid and eutectic tin-lead solder) were studied under both isothermal and non-isothermal conditions. The coupled influence of interfacial Biot number and hydrodynamics on the initiation of phase change was studied.

As seen from the literature review above, the spray cooling is affected by quite a number of parameters. For the spray cooling, the impact velocity (Weber number) is usually quite large, the impact kinetics is dominant, thus the splashing, injection and fingering may happen, which are not desirable in spray cooling. On the contrary, the droplet spray cooling under low impact Weber number is seldom studied, in these cases the capillary force becomes dominant instead of impact kinetics. In this paper we will focus on the droplet spreading under low impact Weber number; the effect of impact velocity, equilibrium contact angle, liquid viscosity, surface tension, droplet radius, thermo-capillary effect, Prandtl number on the droplet spreading and the heat transfer will be studied. In computational modelling of droplet spreading, simulation of moving contact line is one of the main challenges. It has been well established that the dynamic contact angle is not constant during droplet spreading, and it involves different length scales from nanometer to micrometer [15–17]. In the present study, the Molecular Kinetic Theory (MKT) [18] will be adopted to describe the relationship between the dynamic contact angle and velocity of moving contact line. The simulation will be tested by experiments.

In the following sections, the physical model and mathematical formulation with dynamic contact angle model will be introduced first, followed by the validation of current model with our experimental data. After that, the effect of several key parameters of liquid on droplet spreading and the resultant heat transfer is studied. Finally, some conclusions will be drawn for spreading cooling.

2. Physical model and mathematical formulation

In Fig. 1 the schematic diagram of droplet spreading cooling on the hot substrate is shown. When the spherical droplet approaches the solid substrate, the air between the droplet and substrate will be pushed away, the air cushion will be formed no matter how low the droplet approaching velocity is. Firstly, the droplet will skate on the air cushion, usually with a thickness at the order of nanome-

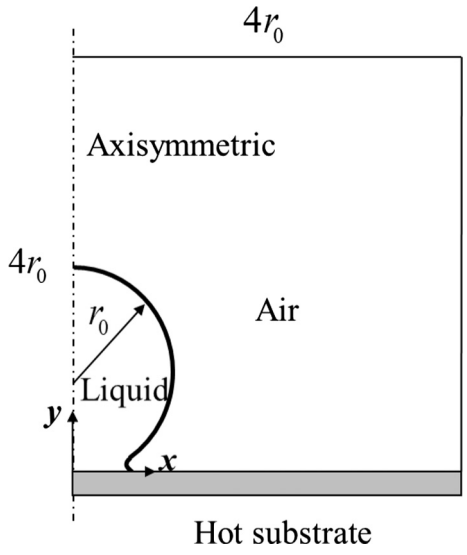

Fig. 1. Schematic diagram and computational domain for droplet spreading on hot substrate (r_0 is the initial droplet radius).

ter, then the bottom of droplet will touch the solid substrate and the droplet starts to spread. According to our experimental observation based on the parameters in our simulation, the skating distance of droplet is between $0.25r_0$ to $0.5r_0$ (r_0 is the initial radius of droplet). In the following simulations, after the sensitivity study of spreading rate on initial skating distance, initial contact angle is set at 165° when the droplet starts to spread, corresponding to the skating distance $0.26r_0$. Due to the difference between the dynamic contact angle and equilibrium contact angle, the contact line will be driven to move along the substrate, the generated capillary wave will propagate along the surface. The droplet spreading can induce the internal flow inside the droplet, and affect the heat transfer between the droplet and substrate. As the approaching velocity of droplet is assumed quite low, the time scale for approaching velocity is larger than that of heat transfer, the uniform temperature gradient is assumed before droplet spreading.

Due to its symmetry, an axisymmetric level set method [19,20] is adopted to simulate the droplet spreading. Under low approaching velocity, the droplet spreading is driven by the capillary force instead of the impact kinetics, hence the capillary-inertial velocity is taken as the characteristic velocity $u_{ci} = \sqrt{\frac{\sigma_0}{\rho_0 r_0}}$. The initial droplet radius is taken as the characteristic length, the temperature difference between the substrate and ambient temperature $T_w - T_0$ is taken as the characteristic temperature. Then the normalized governing equations for two-phase flow are as follows:

Continuity equation

$$\nabla \cdot \vec{u} = 0 \tag{1}$$

Momentum equation

$$\frac{\partial \vec{u}}{\partial t} + \vec{u} \cdot \nabla \vec{u} = -\frac{1}{\rho}\nabla p + \frac{1}{\rho Re}\nabla \cdot [\mu(\nabla \vec{u} + \nabla \vec{u}^T)] + \frac{1 - Ma \cdot T}{\rho Re \cdot Ca}\kappa \vec{n}\delta(\phi) - \frac{Ma}{\rho Re \cdot Ca}\nabla_s T\delta(\phi) \tag{2}$$

Energy equation

$$\frac{\partial T}{\partial t} + \vec{u} \cdot \nabla T = \frac{1}{\rho C_p Re \cdot Pr}\nabla \cdot (\lambda \nabla T) \tag{3}$$

Level Set convection equation

$$\frac{\partial \phi}{\partial t} + \vec{u} \cdot \nabla \phi = 0 \tag{4}$$

The volume fraction is defined with the Heaviside function

$$H_\varepsilon(\phi) = \begin{cases} 0 & \phi < -\varepsilon \\ \frac{1}{2}\left[1 + \frac{\phi}{\varepsilon} + \frac{1}{\pi}\sin\left(\frac{\pi\phi}{\varepsilon}\right)\right] & |\phi| \leqslant \varepsilon \\ 1 & \phi > \varepsilon \end{cases} \tag{5}$$

where

$\varepsilon = 1.5dx$

δ is the Dirac delta function as $\nabla H(\phi)$

The normal vector at the interface

$$\vec{n} = \frac{\nabla \phi}{|\nabla \phi|} \tag{6}$$

The curvature

$$\kappa = \nabla \cdot \frac{\nabla \phi}{|\nabla \phi|} \tag{7}$$

The normalized density, dynamic viscosity, specific heat and thermal conductivity are defined as follows

$$\rho = H + (1 - H)r_d \tag{8a}$$

$$\mu = H + (1 - H)r_\mu \tag{8b}$$

$$C_p = H + (1 - H)r_{Cp} \tag{8c}$$

$$\lambda = H + (1 - H)r_\lambda \tag{8d}$$

Here

$r_d = \rho_g/\rho_l$, $r_\mu = \mu_g/\mu_l$, $r_\lambda = \lambda_g/\lambda_l$, $r_{Cp} = Cp_g/Cp_l$

The governing equations are discretized with a finite volume method on a Marker-And-Cell (MAC) mesh, with velocity defined at cell faces and scalar variables at the cell centers. The coupling between the continuity equation and momentum equation are solved with the standard projection method. The Adams-Bashforth scheme is adopted to solve the advection term, and Crank-Nicolson is adopted to solve the diffusion term. After the intermediate velocity is obtained, it will be updated through pressure correction enforced by continuity equation. For the level set advection equation, the advection term is discretized with a fifth-order Weighted Essentially Non-Oscillatory (WENO) scheme, then the re-initialization algorithm is adopted to keep ϕ as the algebraic distance to the interface. All the spatial discretizations are performed with the second-order central difference scheme.

The dynamic contact angle is described with MKT [18]. In this theory, the dynamic contact angle is defined as the microscopic angle in the first few layers of molecules above the solid wall, and it also equals to the observable angle in the experiment. The dynamic contact angle can be written as the function of velocity of moving contact line as follows:

$$\theta_d = \mathrm{acos}(\cos\theta_w - A\ln(BCa_{cl} + \sqrt{1 + (BCa_{cl})^2})) \tag{9}$$

where $A = \frac{2nk_BT}{\sigma_0}$, $B = \frac{\sigma_0}{2\mu k^2 \lambda}$, and they can be fitted through our experimental data as $A = 0.64$ and $B = 246$.

Due to the symmetry of droplet in y direction, only the right half of droplet is simulated, as seen in Fig. 1. After sensitivity study, the grid size 201×201, the time step 1×10^{-4}, the domain 4×4, the finite slip length $\lambda_s = 1 \times 10^{-5}$ are adopted in the simulation.

The boundary conditions are as follows:

Left boundary ($x = 0$)

Symmetric: $u = 0$, $\frac{\partial v}{\partial x} = 0$, $\frac{\partial T}{\partial x} = 0$

Right boundary ($x = 4$)

Free boundary: $v = 0$, $\frac{\partial u}{\partial x} = 0$, $\frac{\partial T}{\partial x} = 0$

Lower boundary ($y = 0$)

Solid boundary: $u = v = 0$, $T = 1$

Upper boundary ($y = 4$)

Free boundary: $u = 0$, $\frac{\partial v}{\partial y} = 0$, $\frac{\partial T}{\partial y} = 0$

In order to evaluate the relative importance of different forces, the following non-dimensional numbers are defined:

Reynolds number

$$Re = \frac{\rho_l u_{ci} r_0}{\mu_l} \tag{10a}$$

Capillary number

$$Ca = \frac{\mu_l u_{ci}}{\sigma_0} \tag{10b}$$

Weber number

$$We = \frac{\rho_l u_{ci}^2 r_0}{\sigma_0} \tag{10c}$$

Effective Marangoni number

$$Ma = \frac{\sigma_T (T_{drop} - T_w)}{\sigma_0} \tag{10d}$$

Here σ_T is the variation coefficient of surface tension over temperature, and is negative for most liquids.

Ohnsorge number

$$Oh = \frac{\mu_l}{\sqrt{\rho_l \sigma_0 r_0}} \tag{10e}$$

Nusselt number

$$Nu = \lambda \frac{\partial T}{\partial y} \tag{10f}$$

Transient total heat transfer rate

$$q(t) = \int_0^r \lambda \frac{\partial T}{\partial y} dx \tag{10g}$$

The surface tension and viscosity are highly dependent on the temperature, the temperature-dependent surface tension will be studied through the thermo-capillary effect. Due to the low Ohnesorge number, the viscous effect is negligible compared with the inertial effect and capillary effect, hence the temperature-dependent viscosity has little effect on the droplet spreading and heat transfer, this is verified in the preliminary studies. Thus the constant properties are adopted for simulation, which are taken from experiment of water droplet spreading in air as follows:

Liquid density $\rho_l = 988.0\ kg/m^3$, dynamic viscosity $\mu_l = 8.41 \times 10^{-4} Pa{\cdot}s$, surface tension $\sigma_0 = 0.0673\ N/m$, equilibrium contact angle $\theta_0 = 22.2°$, liquid radius $r_0 = 0.365\ mm$. Based on these parameters, the calculated capillary-inertial velocity $u_0 = 0.432\ m/s$, the corresponding non-dimensional numbers $Re = 185.2$, $Oh = 50.4 \times 10^{-3}$, $Ca = 4.69 \times 10^{-3}$, $We = 1.0$, $Pr = 7.0$ and $Ma = 0$.

3. Experiment

In order to validate current numerical model, the experiment on droplet spreading is carried out. The droplet of distilled water is generated from minuscule conical glass nozzles through gravity-driven pinch-off. The substrate is the 1-mm-thick microscope glass slide. For each deposition, a fresh area of the substrate is used, hence there is no liquid film in the deposition area. In order to minimize the effect of droplet kinetics on the droplet spreading, the droplets are deposited onto the substrate with relatively low impact velocity ($We < 0.1$). The rapid spreading is recorded with a Phantom V1610 CMOS high-speed video camera, with frame rates up to 20 k fps. The long-distance microscopes with 10X Mitutoyo objective is used in the camera, with the corresponding pixel resolution of 2.4 μm. Backlighting is accomplished with a 350 W metal-halide lamp (Sumita Optical Glass, Inc), which is shone onto a diffuser. The spreading rates are calculated from the transient variation of measured droplet spreading radius in high-resolution videos.

4. Results and discussion

4.1. Numerical validation

In this study, the relationship between the dynamic contact angle and the velocity of moving contact line is provided with the MKT. In order to test its validity, the transient spreading radius predicted with MKT is compared with that from the model of Constant Contact Angle (CCA) and our experimental data with high-speed camera, as shown in Fig. 2. It can be found that with the CCA model the droplet spreads much faster than that with MKT, because the dynamic contact angle with CCA model is always much lower than that with MKT during the droplet spreading, thus the driving force near the moving contact line is much larger than that predicted with MKT. The transient spreading radius with MKT can agree quite well with the experimental data, and it can also reflect the two distinct spreading stages. One is the capillary-inertial spreading stage, and the other is the capillary-viscous spreading stage. In the early stage upon the droplet deposition, the droplet will spread towards the equilibrium stage, the capillary force will be balanced by the inertial force, thus it is named as capillary-inertial spreading stage. In the later stage, with the slowing down of droplet spreading, the droplet spreading will be balanced by the viscous dissipation, thus it is named as the capillary-viscous spreading stage. This has been studied extensively through experiments and theoretically [21–25]. It is well

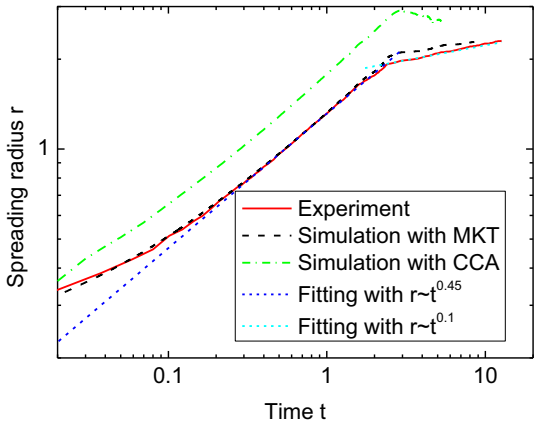

Fig. 2. Comparison of transient variations of spreading radius from experimental and numerical results with Molecular Kinetic Theory (MKT) and Constant Contact Angle (CCA) model for moving contact line. (At this default case, $Re = 185.2$, $Oh = 5.4 \times 10^{-3}$, $Ma = 0$, $Pr = 7.0$).

known that for fast droplet spreading on substrate with fully wetting, in the capillary-inertial spreading stage, the spreading radius r is proportional to $t^{0.5}$. In our study the substrate is partially wetting with equilibrium contact angle $\theta_0 = 22.2^\circ$, the power of time is reduced to 0.45; In the later stage, the droplet spreading is slowed down and transits to the capillary-viscous spreading, the spreading radius is proportional to $t^{0.1}$, this is consistent with the Tanner's law in analytical solution [25]. The comparisons show the accuracy of current numerical model with MKT for moving contact lines.

In Fig. 3 the droplet profiles from numerical simulation and experiment are compared at different times, it can be found that the droplet profile evolution with MKT agrees quite well with the experiment, but the numerical results with CCA deviate greatly from them. Consistent with the results in Fig. 2, the droplet spreads

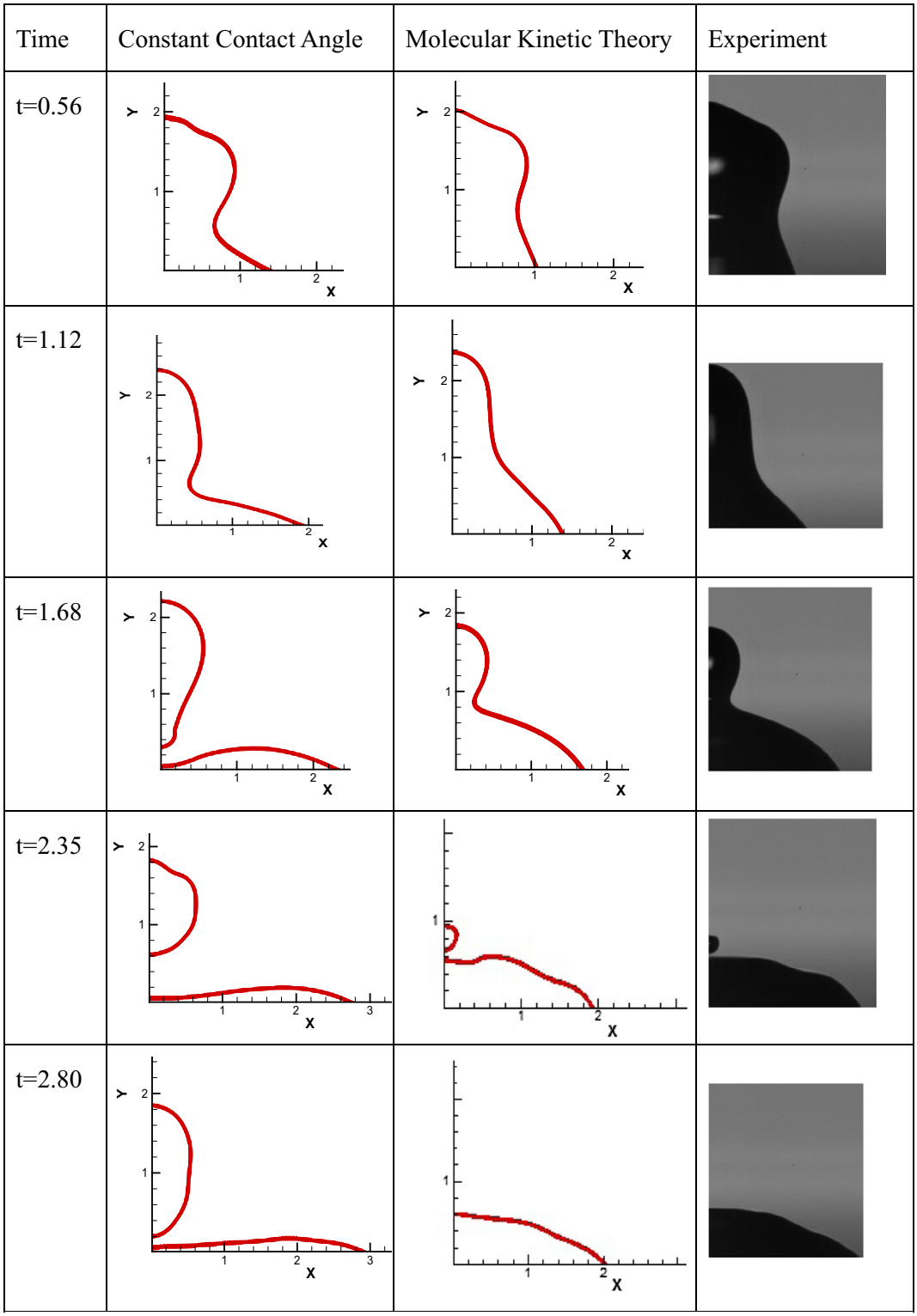

Fig. 3. Transient variations of droplet profiles during droplet spreading for numerical results with Constant Contact Angle model (CCA) and Molecular Kinetic Theory (MKT) for moving contact line, and experiment.

quite fast with CCA. Because the upper region of droplet falls slower than the lower region of droplet, the pinch-off occurs at t = 1.68 and a relatively large droplet is generated. While for the numerical results with MKT and experiment, the pinch-off does not occur at t = 1.68 due to slow spreading rate. Actually, the pinch-off occurs at t = 2.35 when a relatively small droplet is generated. This also proves that the MKT can predict the droplet pinch-off accurately.

4.2. Heat transfer during droplet spreading

The local Nusselt number distributions along the substrate at different times are provided in Fig. 4, it can be found that the heat transfer mainly occurs between the droplet and substrate during droplet spreading, because the heat convection in the droplet is much higher than that in the surrounding gas. During the droplet spreading, the moving contact line will move along the substrate, and the bulk of droplet will move downward towards the substrate, so the impinging flow will be formed inside the droplet. This can be found in the velocity and temperature fields at t = 1.8 in Fig. 5. The local temperature gradient and Nusselt number inside the droplet near the substrate are also high. At t = 2.1 the local Nusselt number reaches the maximum value of 43, then the maximum Nusselt number is decreased due to the slowing down of droplet spreading. At t = 20.0 the Nusselt number becomes very low with nearly uniform distribution, because the droplet has reached the quasi-steady state and heat conduction becomes dominant instead of strong convective heat transfer.

4.3. Effect of impact velocity

The initial impact velocity of droplet can have great effect on the droplet spreading and the heat transfer process, as seen in Fig. 6. When the impact velocity is increased from 0.0375 to 0.432 m/s, the corresponding Weber number based on the impact velocity is increased from 7.53×10^{-3} to 1.0. During the droplet impact on the solid substrate, the impact kinetics can be converted into the spreading kinetics. At low Weber number of 7.53×10^{-3}, the impact kinetics is negligible, the kinetics for spreading mainly comes from the released surface energy; while at high Weber number of 1.0, the impact kinetics becomes significant, and it can be converted into the kinetics for spreading. thus the spreading rate at higher impact velocity is higher, the maximum spreading radius is reached at earlier time. After reaching the maximum spreading radius, the droplet will not spread further in the capillary-viscous spreading stage, and it will approach steady stage with almost constant spreading radius.

During the droplet spreading at high impact velocity, the flow inside the droplet becomes stronger, resulting in stronger convective heat transfer between the droplet and solid substrate, thus the heat flux at high impact velocity is higher than that at low impact velocity in the capillary-inertial spreading stage. Because the droplet spreads little at the later capillary-viscous spreading stage, its total heat transfer rate will not increase dramatically at high impact velocity. On the contrary, at low impact velocity, the droplet will continue to spread in the capillary-viscous spreading stage, its total heat transfer will increase sharply at the transition point from the capillary-inertial spreading stage to capillary-viscous spreading stage. Although the impact velocity of 0.432 m/s is one order higher than that of 0.0375 m/s, there is not significant heat transfer enhancement, this can be explained from the variation of dynamics contact angle, as seen in Fig. 6(c). According to Eq. (9) from MKT, the dynamic contact angle is increased with the increasing velocity of moving contact lines. At high impact velocity $u_0 = 0.432$ m/s, the velocity of moving contact lines is higher than that at low velocity $u_0 = 0.0375$ m/s, hence the dynamic contact angle is also higher. Because higher dynamic contact angle can impede the droplet spreading, the ratio of droplet spreading rate is not as high as the ratio of impact velocity. It can also be noted that when the droplet reaches the maximum spreading radius, the velocity of moving contact lines will approach zero, leading to the sharp decrease of dynamic contact angle.

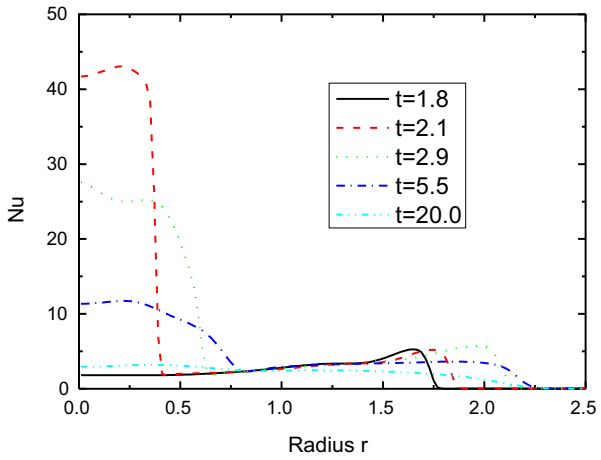

Fig. 4. Local Nusselt number distribution along the substrate for droplet spreading at different times. (Re = 185.2, $Oh = 5.4 \times 10^{-3}$, Ma = 0, Pr = 7.0).

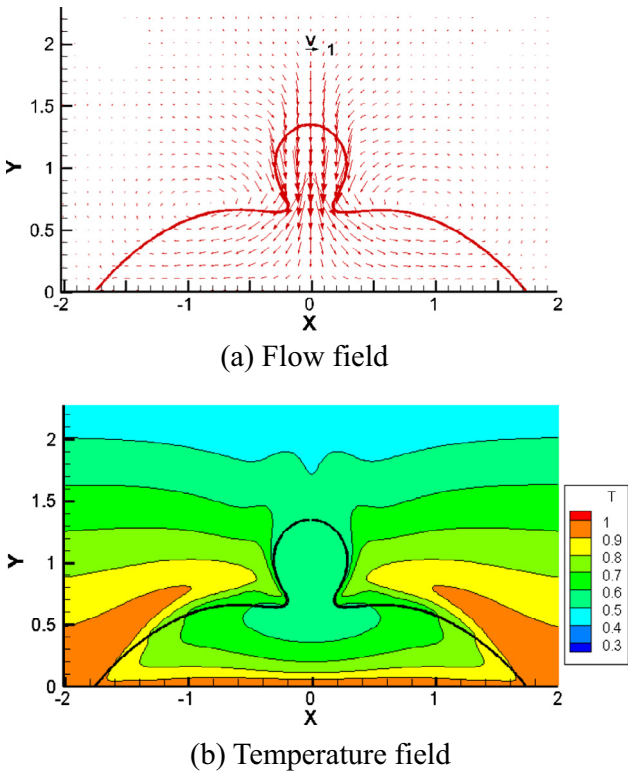

Fig. 5. Velocity and temperature fields during droplet spreading at t = 1.8 (Re = 185.2, $Oh = 5.4 \times 10^{-3}$, Ma = 0, Pr = 7.0).

4.4. Effect of equilibrium contact angle

Due to the surface roughness or chemical property, the substrates may have different values of equilibrium contact angle,

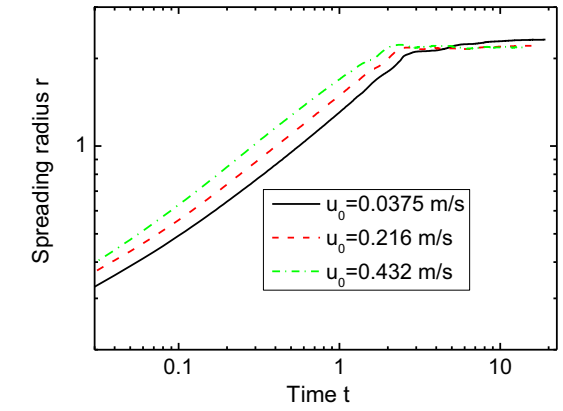

(a) Spreading radius

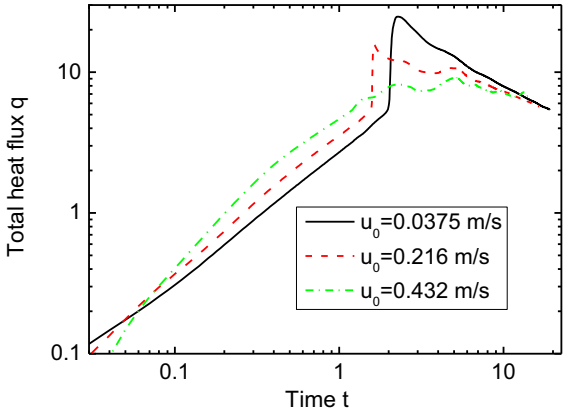

(b) Heat flux

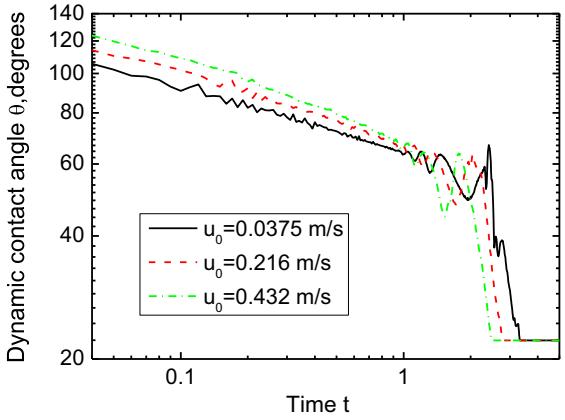

(c) Dynamic contact angle

Fig. 6. Effect of impact velocity on spreading radius, heat flux and dynamic contact angle ($Oh = 5.4 \times 10^{-3}$, $Ma = 0$, $Pr = 7.0$; The corresponding Reynolds number $Re = 16.08$ at $u_0 = 0.0375$ m/s; $Re = 92.62$ at $u_0 = 0.216$ m/s; $Re = 185.2$ at $u_0 = 0.432$ m/s).

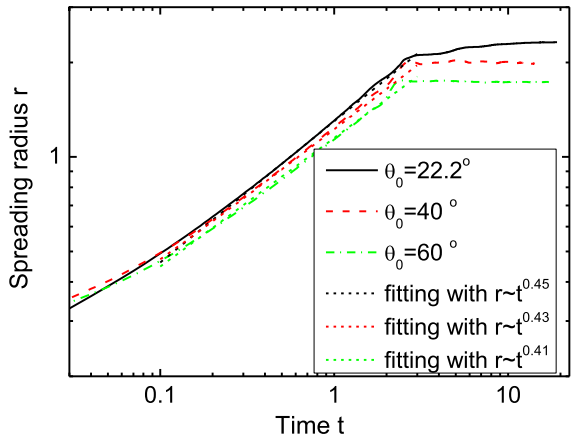

(a) Spreading radius

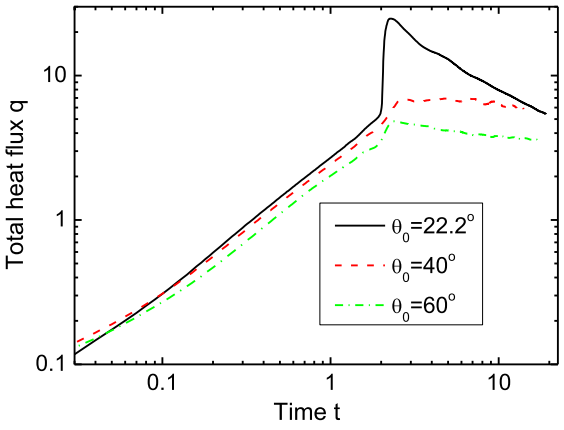

(b) Heat flux

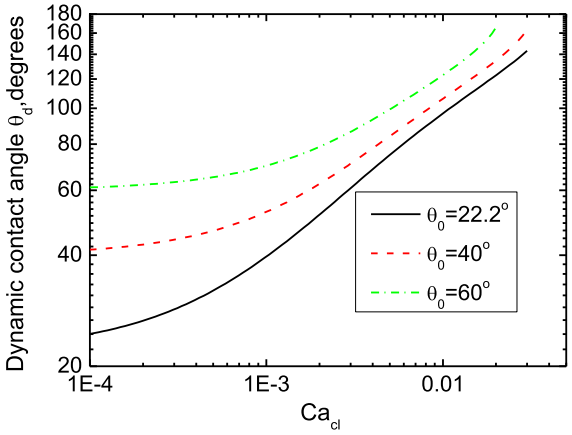

(c) Dynamic contact angle

Fig. 7. Effect of droplet equilibrium contact angle on spreading radius and total heat flux ($Re = 185.2$, $Oh = 5.4 \times 10^{-3}$, $Ma = 0$, $Pr = 7.0$).

which can also affect the droplet spreading. The relationship between dynamic contact angle and velocity of moving contact line is described with MKT. When the equilibrium contact angle is increased, the dynamic contact angle will also be increased under the same velocity of moving contact line, as seen in Fig. 7 (c). When the equilibrium contact angle is increased from 22.2° to 60°, the droplet spreading rate is decreased because the driving force is determined by the difference between the dynamic contact angle and equilibrium contact angle. As the Ohnesorge number is quite low at 5.4×10^{-3}, the droplet spreading is the capillary-inertial spreading, with the spreading radius over time following the scaling law. It is well known that on the fully wetting substrate with zero equilibrium contact angle, the spreading radius r over time follows $r \sim t^{0.5}$.From Fig. 7(a), it can be found that the power is decreased to 0.45, 0.43 and 0.41 when the equilibrium contact angle is increased from 22.2°, 40° to 60°. The power 0.41 at 60° is quite close to 0.40 in their correlation obtained by Bird et al. [24]. As expected, at high equilibrium contact angle, the equilib-

rium contact radius is decreased because the overall droplet volume is constant.

Because stronger flow can be induced inside the droplet at lower equilibrium contact angle, the peak heat flux at low equilibrium contact angle is higher than that of high equilibrium contact angle. The peak heat flux occurs near the transition point when the capillary-inertial spreading transits to capillary-viscous spreading stage.

4.5. Effect of liquid viscosity

The liquid viscosity has great effect on the droplet spreading and the heat transfer, as shown in Fig. 8. When the liquid viscosity is increased from 8.41×10^{-4} to 0.01 Pa·s, the corresponding Ohnesorge number is increased from 0.0054 to 0.064, the spreading rate at low viscosity is much faster than that of high viscosity. Furthermore, at liquid viscosity $\mu_l = 8.41 \times 10^{-4}$Pa·s, the droplet spreading can be divided into the capillary-inertial spreading stage and capillary-viscous spreading stage clearly, while at large liquid viscosity $\mu_l = 0.01$ Pa · s, the transition between two stages becomes quite smooth. It is also noted that in the initial capillary-inertial spreading stage, the heat flux is increased gradually because the induced flow inside the droplet becomes stronger. Near the critical transition point at around $t = 2.1$, the heat flux reaches the maximum and starts to decrease because the flow is suppressed by viscosity in the capillary-viscous spreading stage. When the liquid viscosity is increased from 8.41×10^{-4} to 0.01 Pa · s, the maximum heat flux is decreased sharply from 17.9 to 1.33, and the average heat flux is also decreased greatly.

4.6. Effect of surface tension

The kinetics for droplet spreading comes from the energy stored as surface tension. When the droplet is deposited on the substrate, it will deform towards the equilibrium stage. Due to the reduction of surface area of droplet, the surface energy will be released and converted into droplet kinetics, hence the surface tension can affect the droplet spreading. From Fig. 9(a), it can be found that at high surface tension $\sigma_0 = 0.1$ N/m, the droplet spreads quite fast due to the high capillary force, and it reaches the maximum spreading radius at the end of capillary-inertial spreading stage, and comes to rest quickly. The corresponding total heat transfer will increase steadily, after reaching the maximum value it will start to decrease quickly. On the contrary, when the surface tension is low at $\sigma_0 = 0.02$ N/m, the driven capillary force will become quite weak, the droplet spreads mildly in both capillary-inertial spreading stage and capillary-viscous spreading stage. The corresponding total heat transfer rate will be quite low, and it increases mildly in the capillary-inertial spreading stage, then decreases a

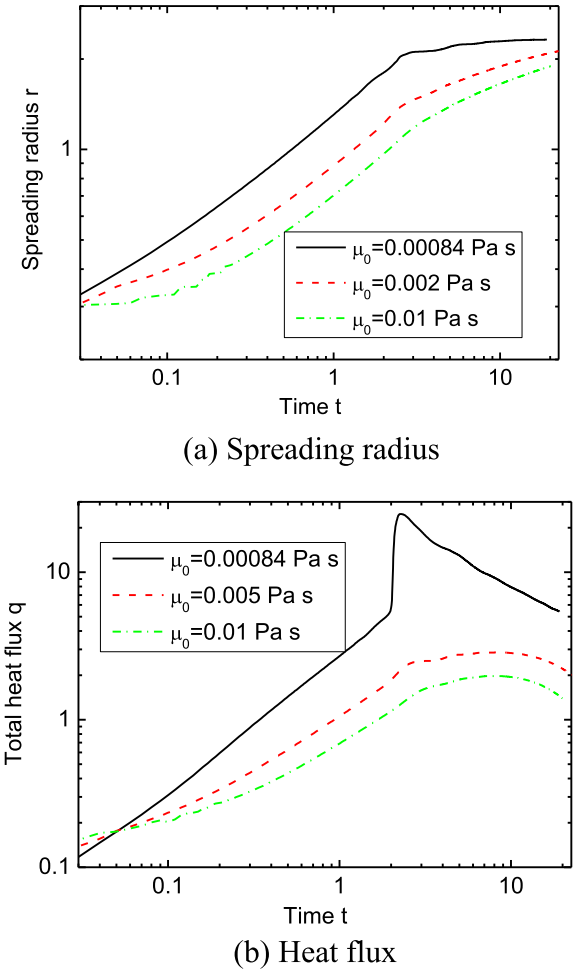

Fig. 8. Effect of droplet viscosity on spreading radius and total heat flux ($Ma = 0$, $Pr = 7.0$; The corresponding Reynolds numbers and Ohnesorge numbers are $Re = 185.2$, $Oh = 50.4 \times 10^{-3}$ at $\mu_l = 8.41 \times 10^{-4}$Pa · s; $Re = 31.2$, $Oh = 0.0321$ at $\mu_l = 0.002$ Pa · s; $Re = 15.6$, $Oh = 00.0642$ at $\mu_l = 0.01$ Pa · s).

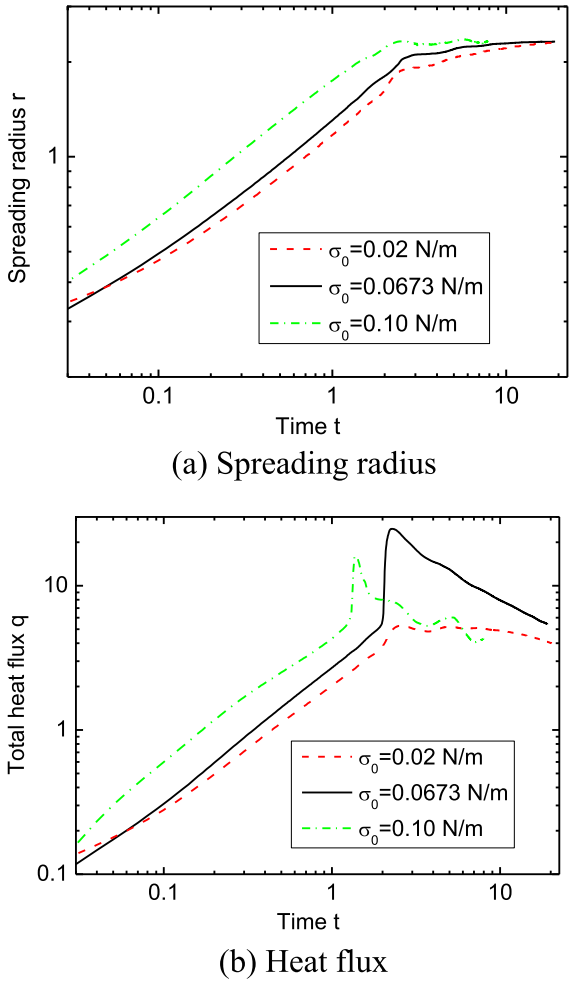

Fig. 9. Effect of surface tension on spreading radius and total heat flux ($Ma = 0$, $Pr = 7.0$; The corresponding Reynolds numbers and Ohnesorge numbers are $Re = 101$, $Oh = 90.90 \times 10^{-3}$ at $\sigma_0 = 0.02$ N/m; $Re = 185.2$, $Oh = 50.4 \times 10^{-3}$ at $\sigma_0 = 0.0673$ N/m; $Re = 225.8$, $Oh = 40.43 \times 10^{-3}$ at $\sigma_0 = 0.1$ N/m).

little at the capillary-viscous spreading stage. When the surface tension is intermediate at $\sigma_0 = 0.0673$ N/m, the maximum total heat transfer rate is reached, and it is also highest at the capillary-viscous spreading stage.

4.7. Effect of initial droplet radius

Fig. 10 shows the effect of initial droplet radius on the droplet spreading rate. Within the radius range from 0.1 to 0.75 mm, the Ohnesorge number is less than 0.01 and the Bond number is less than 0.08, hence the viscous effect and gravitational effect can be neglected. It can be found that with the increasing droplet radius, the spreading rate increases slightly, finally it will approach the constant equilibrium radius. The heat flux at $r_0 = 0.365$ mm is quite close to $r_0 = 0.75$ mm due to the close spreading rate, but the heat flux at $r_0 = 0.1$ mm is much lower due to its lower spreading rate.

4.8. Effect of thermo-capillary force

It is well known that the surface tension of liquid depends on the temperature, hereby it is assumed that the variation of surface tension is inversely related to that of the temperature, as shown by most liquids. Due to the temperature variation along the surface, the tangential force will be generated, which can induce the tangential thermo-capillary force along the surface, and affect the droplet spreading and heat transfer. The strength of the thermo-capillary effect can be reflected by effective Marangoni number in Eq. (10d).

If the substrate temperature is lower than droplet temperature $T_w < T_l$ ($Ma < 0$), and resultant thermal-capillary force will act downward along the droplet surface. Because the direction of thermal-capillary force is consistent with the spreading direction, it will promote the droplet spreading, thus the heat transfer is also promoted. On the contrary, if the substrate temperature is higher than droplet temperature $T_w > T_l$ ($Ma > 0$), it will retard the droplet spreading, and heat transfer is weakened, as seen in Fig. 11.

4.9. Effect of Prandtl number

The effect of Prandtl number on the heat transfer performance during droplet spreading is provided in Fig. 12, here it is assumed that the thermo-capillary force is absent, hence flow is not affected by the temperature field, the transient variation of spreading radius under different Prandtl numbers are identical, thus it will not be provided here. It can be found that during the capillary-inertial spreading stage, Prandtl number has slight effect on the heat transfer performance. Because during the capillary-inertial spreading stage the typical time scale for heat transfer is longer than that of droplet spreading, the temperature field inside the droplet has not been greatly changed. While when the droplet reaches the capillary-viscous spreading stage, the heat flux under large Prandtl number is much higher than that under low Prandtl numbers.

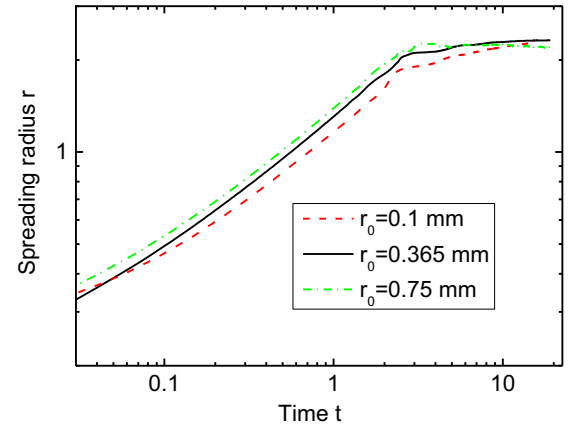

(a) Spreading radius

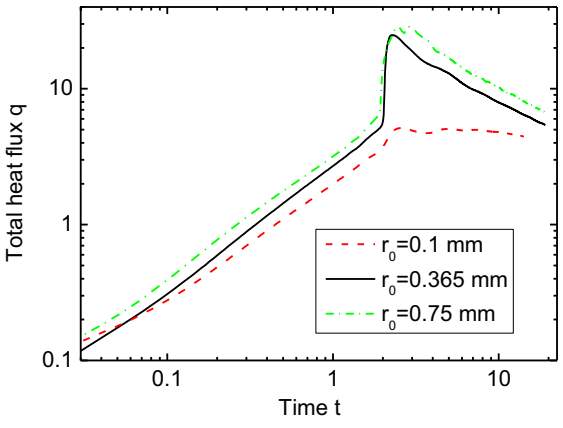

(b) Heat flux

Fig. 10. Effect of droplet radius on spreading radius and total heat flux ($Ma = 0$, $Pr = 7.0$; The corresponding Reynolds numbers and Ohnesorge numbers are $Re = 97.0$, $Oh = 10.03 \times 10^{-2}$ at $r_0 = 0.1$ mm; $Re = 185.2$, $Oh = 50.4 \times 10^{-3}$ at $r_0 = 0.365$ mm; $Re = 265.5$, $Oh = 30.77 \times 10^{-3}$ at $r_0 = 0.75$ mm).

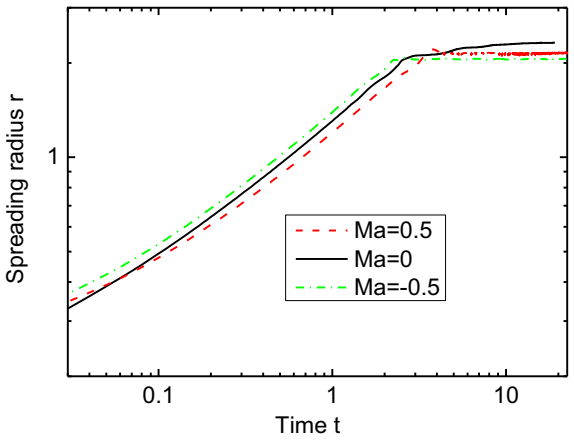

(a) Spreading radius

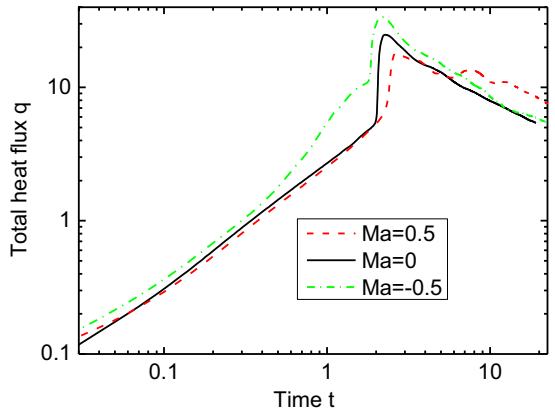

(b) Heat flux

Fig. 11. Effect of thermo-capillary force on spreading radius and total heat flux ($Re = 185.2$, $Oh = 5.4 \times 10^{-3}$, $Pr = 7.0$).

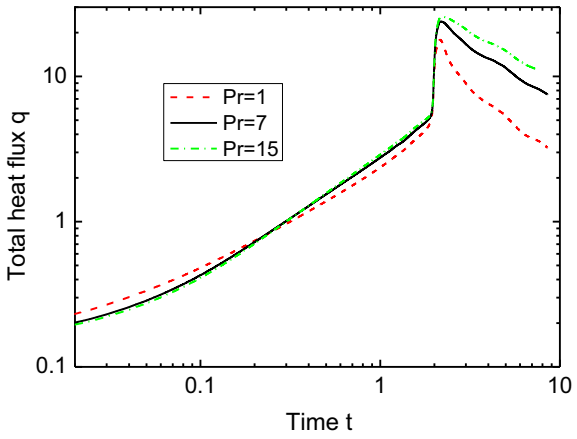

Fig. 12. Effect of *Pr* number on total heat flux (Re = 185.2, $Oh = 5.4 \times 10^{-3}$, Ma = 0).

5. Conclusion

The droplet spray cooling on hot substrates is investigated through transient two-dimensional axisymmetric level set method, the dynamics of moving contact line is described with MKT with fitting parameters from the experimental data. The effect of impact velocity, equilibrium contact angle, liquid viscosity, surface tension, initial droplet radius, thermo-capillary force, Prandtl number on the droplet spreading and heat transfer is studied, the following conclusions are drawn.

(1) The dynamics of moving contact line can be described accurately with MKT, while CCA model can overpredict the droplet spreading rate.
(2) In the initial capillary-inertial spreading stage, the heat transfer increases sharply. It reaches the maximum at the transition point when the capillary-inertial spreading transits to capillary-viscous spreading, then it will decrease mildly.
(3) The droplet spreading radius over time follows the power law, and the power is related to the equilibrium contact angle. When the equilibrium contact angle is increased from 22.2° to 60°, the power exponent is decreased from 0.45 to 0.41.
(4) The droplet spreading rate will increase with increasing impact velocity, surface tension and initial radius, or decreasing equilibrium contact angle and liquid viscosity.
(5) Due to the effect of thermo-capillary effect, if the variation of surface tension is inversely related to that of the temperature, the cold substrate can promote the droplet spreading and the hot substrate can retard the droplet spreading.

Conflict of interest

The authors declared that there is no conflict of interest.

Acknowledgement

This work was financially supported by the Natural Science Foundation of China (Grant Nos: 51406050 and 51436004), The Natural Science Foundation of Beijing (Grant No: 3162029), Marie Curie European Fellowship (Grant No. 658437) and the Fundamental Research Funds for the Central Universities (Grant No. JB2015RCY01).

References

[1] J.H. Kim, Spray cooling heat transfer: the state of the art, Int. J. Heat Fluid Flow 28 (2007) 753–767.
[2] E. Berberović, I.V. Roisman, S. Jakirlić, C. Tropea, Inertia dominated flow and heat transfer in liquid drop spreading on a hot substrate, Int. J. Heat Fluid Flow 32 (2011) 785–795.
[3] B. Basinger, G. Aguilar, J.S. Nelson, Effect of skin indentation on heat transfer during cryogen spray cooling, Laser. Surg. Med. 34 (2004) 155–163.
[4] S. Semenov, A. Trybala, R.G. Rubio, N. Kovalchuk, V. Starov, M.G. Velarde, Simultaneous spreading and evaporation: recent developments, Adv. Colloid Interface Sci. 206 (2014) 382–398.
[5] W.M. Healy, J.G. Hartley, S.I. Abdel-Khalik, On the validity of the adiabatic spreading assumption in droplet impact cooling, Int. J. Heat Mass Transf. 44 (2001) 3869–3881.
[6] M. Pasandideh-Fard, S.D. Aziz, S. Chandra, J. Mostaghimi, Cooling effectiveness of a water drop impinging on a hot surface, Int. J. Heat Mass Transf. 22 (2001) 201–210.
[7] J.H. Moon, M. Cho, S.H. Lee, Dynamic wetting and heat transfer characteristics of a liquid droplet impinging on heated textured surfaces, Int. J. Heat Mass Transf. 97 (2016) 308–317.
[8] J.H. Moon, M. Cho, S.H. Lee, Spreading and receding characteristics of a non-Newtonian droplet impinging on a heated surface, Exp. Therm Fluid Sci. 57 (2014) 94–101.
[9] S. Ganesan, J. Venkatesan, S. Rajasekaran, Modeling of the non-isothermal liquid droplet impact on a heated solid substrate with heterogeneous wettability, Int. J. Heat Mass Transf. 88 (2015) 55–72.
[10] J. Venkatesan, S. Rajasekaran, A. Das, S. Ganesan, Effects of temperature-dependent contact angle on the flow dynamics of an impinging droplet on a hot solid substrate, Int. J. Heat Fluid Flow 62 (2016) 282–298.
[11] A.J. Díaz, A. Ortega, Investigation of a gas-propelled liquid droplet impinging onto a heated surface, Int. J. Heat Mass Transf. 67 (2013) 1181–1190.
[12] G. Strotos, M. Gavaises, A. Theodorakakos, G. Bergeles, Numerical investigation of the cooling effectiveness of a droplet impinging on a heated surface, Int. J. Heat Mass Transf. 51 (2008) 4728–4742.
[13] G. Strotos, G. Aleksis, M. Gavaises, K.S. Nikas, N. Nikolopoulos, A, Theodorakakos, Non-dimensionalisation parameters for predicting the cooling effectiveness of droplets impinging on moderate temperature solid surfaces, Int. J. Therm Sci 50 (2011) 698–711.
[14] R. Bhardwaj, J.P. Longtin, D. Attinger, A numerical investigation on the influence of liquid properties and interfacial heat transfer during microdroplet deposition onto a glass substrate, Int. J. Heat Mass Transf. 50 (2010) 2912–2923.
[15] S. Ganesan, On the dynamic contact angle in simulation of impinging droplets with sharp interface methods, Microfluid. Nanofluid 14 (2013) 615–625.
[16] W. Ren, E. Weinan, Boundary conditions for the moving contact line problem, Phys. Fluids 19 (2007) 65.
[17] Y. Sui, H. Ding, P.D.M. Spelt, Numerical simulations of flows with moving contact lines, Ann. Rev. Fluid Mech. 46 (2014) 97–119.
[18] D. Duvivier, T.D. Blake, C.J. De, Toward a predictive theory of wetting dynamics, Langmuir 29 (2013) 10132–10140.
[19] Y. Sui, Moving towards the cold region or the hot region? Thermocapillary migration of a droplet attached on a horizontal substrate, Phys. Fluids 26 (2014) 092102.
[20] Y. Sui, P.D.M. Spelt, Non-isothermal droplet spreading/dewetting and its reversal, J. Fluid Mech. 776 (2015) 74–95.
[21] P.G. De Gennes, Wetting: statics and dynamics, Rev. Mod. Phys. 57 (1985) 827–863.
[22] D. Bonn, J. Eggers, J. Indekeu, J. Meunier, E. Rolley, Wetting and spreading, Rev. Mod. Phys. 81 (2009) 739–805.
[23] A.L. Biance, C. Clanet, D. Quere, First steps in the spreading of a liquid droplet, Phys. Rev. E 69 (2004) 016301.
[24] J.C. Bird, S. Mardre, H.A. Stone, Short-time dynamics of partial wetting, Phys. Rev. Lett. 100 (2008) 234501.
[25] L. Tanner, The spreading of silicone oil drops on horizontal surfaces, J. Phys. D Appl. Phys. 12 (1979) 1473–1484.